

Fluorescence-lifetime identification of biological agents using deep ultraviolet light-emitting diodes

P. Vitta^a, N. Kurilčik^a, S. Juršėnas^a, A. Žukauskas^a, E. Bakienė^b, J. Zhang^c, T. Katona^c, Y. Bilenko^c,
A. Lunev^c, X. Hu^c, J. Deng^c, and R. Gaska^c

^aInstitute of Materials Science and Applied Research, Vilnius University,
Saulėtekio 9-III, LT-10222 Vilnius, Lithuania

^bDepartment of Biochemistry and Biophysics, Vilnius University,
M. K. Čiurlionio 21/27, LT-03101 Vilnius, Lithuania

^cSensor Electronic Technology, Inc., 1195 Atlas Road, Columbia, SC 29209 USA

ABSTRACT

Recently developed deep-UV light-emitting diodes (LEDs) are already used in prototype fluorescence sensors for detection of hazardous biological agents. However, increasing of the sensor ability of discrimination against common interferents requires further development of measurement technique. In particular, LED-based fluorescence lifetime measurements are to be considered as a technique supplementary to fluorescence spectral and excitation measurements. Here we report on application of UVTOP[®] series deep-UV LEDs developed by Sensor Electronic Technology, Inc. for real-time measurements of fluorescence lifetime in the frequency domain. LEDs with the wavelengths of 280 nm (targeted to protein excitation) and 340 nm (for excitation of coenzymes NADH and flavins) were used. The output of the LEDs was harmonically modulated at frequencies up to 100 MHz and fluorescence lifetime on the nanosecond and subnanosecond scale was estimated by measuring the phase angle of the fluorescence signal in respect of the LED output. Dual-wavelength LED-based phase-resolved measurement technique was tested for discrimination of *B. globigii* against a variety of interferents such as diesel fuel, paper, cotton, dust, etc. We conclude that fluorescence phase measurements have potential to improve the discrimination ability of the “detect-to-warn” optical bioparticle sensors.

Keywords: UV LEDs, fluorescence lifetime, frequency domain, *B. globigii* spores

1. INTRODUCTION

Nowadays, the need of a sensitive sensor for real-time detection of chemical and biological agents increases because of increasing threats of attacks using biological warfare agents from terrorist nets and rogue political regimes. Such “detect-to-warn” devices must be compact, cost-efficient, low-maintenance, fast and with high probability of detection of hazardous agents with low false alarm rate. Optically based methods of chemical and biological sensing offer fast and *in situ* detection and preliminary identification of hazardous agents.¹ A variety of techniques, such as elastic and inelastic scattering of light, absorbance, fluorescence, and breakdown emission spectroscopy, can be employed.² In particular, measurements of spectral and excitation characteristics of fluorescence excited by UV radiation is already a well established technique for detect-to-warn sensors of airborne bioparticles.

Historically, laser induced fluorescence (LIF) mostly based on ion, excimer, and solid-state lasers is a well-developed analytical technique with a fast response, high spatial resolution, and ability of remote sensing.^{3,4} In particular, sophisticated systems employing advanced solid-state lasers with parametric converters for tailoring the UV wavelengths with the excitation spectra of biofluorophores and equipped with multichannel spectral analyzers can provide with extended spectroscopic data on fluorescence of various biological agents and interferents.⁵ However despite the crucial role of gas-discharge and solid-state lasers in analytical spectroscopy, these devices still remain quite expensive, heavy, and bulky sources of light with high power consumption and high maintenance. Meanwhile for continuous monitoring of large areas for protection of both military and civilian populations, optical sensors on demand must meet strict requirements on reduced size, weight, cost, power consumption, and maintenance.

As one of the possible alternatives, UV emission for “detect-to-warn” sensors with early warning capability can be generated by light-emitting diodes (LEDs), which are inexpensive, compact, lightweight, and low-maintenance semiconductor emitters. Recently, semiconductor-based sources of UV light became available owing to a tremendous progress in nitride semiconductor technology.⁶ In particular, UV LEDs and laser diodes (LDs) are being developed based on $\text{Al}_x\text{Ga}_{1-x}\text{N}$ alloy, which can be tailored for wavelengths ranging from 360 to 200 nm depending on Al molar fraction x . This wavelength range exactly matches the excitation spectra of most important natural autofluorophores contained in biological agents, such as bacteria, spores, and viruses. Although suffering from low coherence length that is insufficient for obtaining high density of optical power for single-particle interrogation and remote sensing, LEDs are already used in numerous prototype sensor systems.^{7–10}

An important issue to be addressed in the developing of optical detect-to-warn sensors is the increasing of the discrimination ability, which is of crucial importance for decreasing of the false alarm rate of a detector. Up to now, the discrimination ability of the most advanced compact biofluorescence sensors was based on differential schemes employing two fluorescence signals invoked by two excitation sources, typically operating at 280 nm and 340 nm wavelengths, which allow for the photoexcitation of aromatic amino acids (tyrosine and tryptophan) and coenzymes (NADH and flavins), respectively.^{11,12} However, despite optimal discrimination algorithms employed, cost-efficient systems with low number of detection channels still suffer from an overlap of data originated from hazardous bioagents with those from numerous background interferents, such as dust, particles of paper, fiber, and food, aromatic hydrocarbons (typically particles of diesel fuel), pollen, fungi, etc. To that end, introduction of an additional dimension of optical discrimination is highly desirable. In particular, laser-induced breakdown emission and deep-UV Raman spectroscopy was considered.^{13,14} Meanwhile, spectral and excitation autofluorescence signatures can be supplemented by a third dimension of fluorescence, fluorescence decay time (fluorescence lifetime), which is a unique fingerprint of a fluorophore. Since measurements of fluorescence lifetime can be performed using the same excitation and detection optical set-up, introduction of such an additional dimension in fluorescence measurements can require only improvements in the electronic circuit of a detector with a minor increase in price.

Basically, fluorescence lifetime measurements can be carried out in two ways.¹⁵ The first one, which is widely used in spectroscopy and practical applications, is based on short-pulse excitation with subsequent tracing of temporal distribution of fluorescence (time-domain measurement). The second, alternative, approach is based on using of harmonically modulated excitation and measuring of the phase shift and/or decrease in the modulation depth of the fluorescence signal (frequency-domain measurement). Time-domain measurements can be conducted for levels of fluorescence as low as discontinuous single-photon fluxes (e.g., using time-correlated photon counting technique), however numerous data points are to be acquired and the data are to be numerically processed. Contrarily, frequency-domain technique enables one to acquire the decay-time signature from a single measurement, what is preferable for cost-efficient detectors operating in real-time regime. Correspondingly, the price paid is a lower sensitivity, since usually the harmonic component can be unambiguously extracted only from a continuous signal.

Soon after the development of bright blue and near-UV LEDs, cost-efficient fluorescence lifetime measurements in some chemical compounds were demonstrated in both subnanosecond-pulse¹⁶ and harmonic modulation regimes.¹⁷ Recently, deep-UV LEDs were applied for fluorescence lifetime measurements in biological compounds and agents.^{18–22} In particular, real-time frequency-domain measurements were implemented in four basic bacterial-spore biofluorophores³ (aromatic amino acids tyrosine and tryptophan as well as coenzymes NADH and riboflavin) using 280-nm and 340-nm LEDs.²²

In this work, we present our recent data on application of the currently most advanced deep-UV LEDs developed by Sensor Electronic Technology, Inc. (SET Inc.) for fluorescence discrimination of *B. globigii* spores (simulant of hazardous biological agent *B. anthracis*) against common airborne interferents. After description of the experimental technique (Section 2), we present results on conventional two-channel spectral and excitation fluorescence discrimination using 280-nm and 340-nm LEDs (Section 3). In Section 4 we introduce the third fluorescence discrimination dimension, fluorescence lifetime measurements in the frequency domain. We conclude that fluorescence lifetime measurements can improve the discrimination ability of detect-to-warn sensors of airborne bioparticles (Section 5).

2. EXPERIMENTAL

2.1 Deep UV LEDs

Deep UV LEDs used in this study have been developed at SET, Inc. under support from Defense Advanced Research Project Agency (Program Manager Dr. J. Carrano). Detailed information on 340-nm and 280-nm LEDs design and growth procedures is presented in Refs. 23–26. The LED structures were grown on basal plane sapphire substrates in a custom-designed vertical metalorganic chemical vapor deposition (MOCVD) system, with trimethylaluminum, trimethylgallium, silane, Cp_2Mg , and NH_3 as precursors. The high quality AlN buffer and AlGaIn-based superlattices for strain management were grown using a Migration Enhanced MOCVD (MEMOCVDTM) technique. Optimization of MEMOCVD growth yielded high-quality AlN buffers and AlN/AlGaIn superlattices with the full width at half maximum ≤ 9 arcsec for AlN x-ray diffraction (0002) ω -scan. LED patterns with various area/perimeter ratios were designed and mesa type devices were fabricated. Flip-chip packaging with massive contact bumps was used for light extraction through a UV-transparent sapphire substrate and efficient heat removal. Continuous wave power of the 340 nm LEDs was up to 0.6 mW at 30 mA (wall-plug efficiency 0.3%) and up to 1 mW at 20 mA for 280 nm LEDs (wall-plug efficiency 0.9%). The emission spectra revealed a 10-nm full width at a half magnitude line width and a low long-wavelength background-to-peak intensity ratio of approximately 0.01% when measured at a wavelength 70-nm larger than the peak wavelength (e.g., at 350 nm for 280 nm LEDs).²⁰ The harmonic-modulation characteristics of the UV LEDs exhibited cut-off frequencies of about 80 MHz and 130 MHz for the 340-nm and 280-nm LEDs.²⁰

2.2 Experimental set-up

For conventional measurements of fluorescence spectra, 340-nm and 280-nm LEDs equipped with shortpass filters (SPFs) described below were used. The spectra were resolved using a low-stray-light double monochromator (JY HRD1) and recorded using a photomultiplier (PMT) operating in the photon counting mode (Hamamatsu R1463P). The experimental set-up used for frequency-domain fluorescence measurements is depicted in Fig. 1.

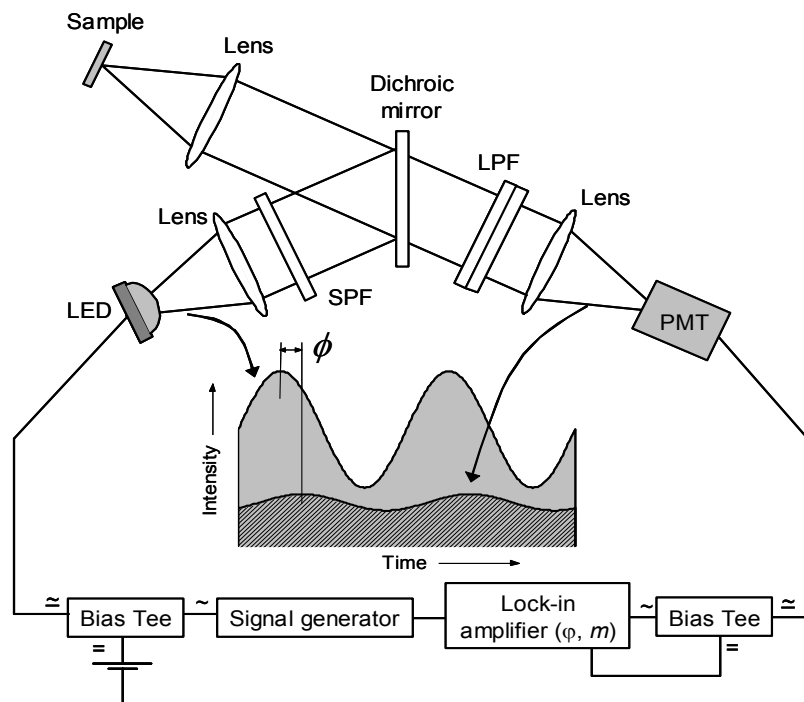


Fig. 1. Optical scheme and block diagram of the experimental set-up for frequency-domain fluorescence lifetime measurements.

An LED (either 340-nm or 280-nm) was driven using a bias tee (Picosecond 5547). The bias current was 30 mA and radio-frequency modulation of +15 dbm (32 mW) was provided by a high-power signal generator (Aeroflex

IFR 2023A). After collimation by a fused-silica lens, the emission was passed through an SPF to remove the long-wavelength residual radiation of the AlGaIn structure. A Schott UG11 glass or a custom made interference filter with a cut-off wavelength of 285 nm were used for 340-nm and 280-nm LEDs, respectively. The filtered emission of an LED was reflected by a custom made dichroic mirror with the transition wavelength of 395 nm or 295 nm for 340-nm and 280-nm LEDs, respectively, and focused to a sample using a second fused-silica lens. The latter lens simultaneously was used for collimation of fluorescence, which was passed through the dichroic mirror and a longpass filter (LPS). The LPS was stacked of glass and/or interference filters. For measurements using 340-nm LED, Schott BG18 and GG420 glass filters were used, whereas for 280-nm LED, the stack contained a custom made interference filter with a cut-off wavelength of 320 nm and a Schott BG24 glass filter. All custom-made dichroic mirrors and interference filters were manufactured by Optida Ltd., Vilnius. Figures 2a and b depict the spectral power distribution of the LEDs' emission incident on sample (solid lines) and the transmittance of the detection arm for measurements using 340-nm and 280-nm LEDs, respectively.

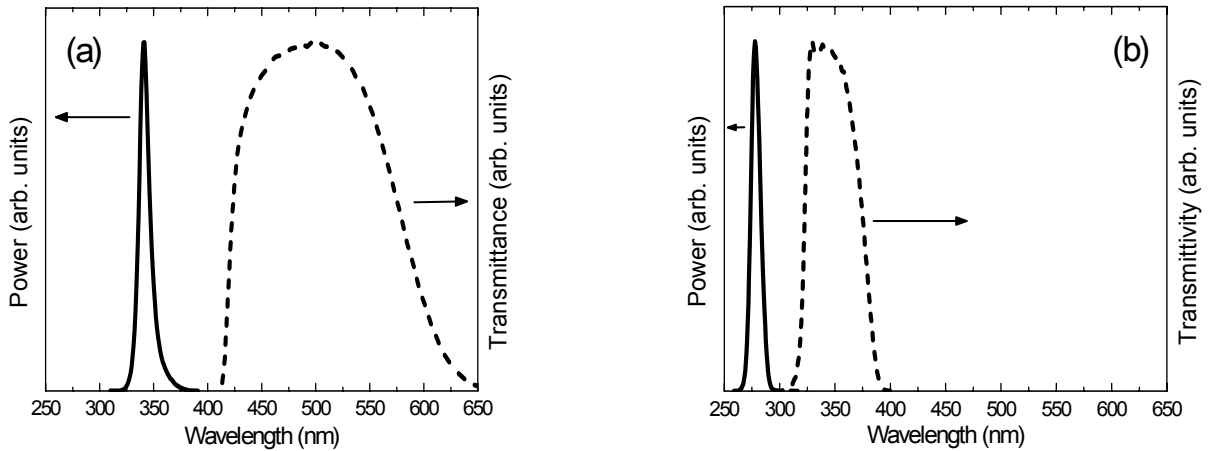


Fig. 2. Spectral power distribution of UV radiation incident on sample (solid lines) and transmittance of the detection arm (dashed lines) for measurement set-up using 340-nm (a) and 280-nm (b) LEDs.

After filtering, the fluorescence was focused on the cathode of a photomultiplier (PMT) with a subnanosecond risetime (Hamamatsu H6780-01). The electrical signal from the PMT was branched into ac and dc components using a second bias tee. These components were fed into a radio-frequency lock-in amplifier (Stanford Research Systems SR844) and used for measurement of the phase and modulation depth of the fluorescence.²⁷

Use of a harmonically modulated source for fluorescence excitation allows for measurement of fluorescence lifetime by simple comparison between the excitation and fluorescence signals phase and modulation depth.¹⁵ The principle of the frequency-domain measurement is illustrated in the insert of Fig. 1. The excitation source is modulated by a harmonic (sinusoidal) waveform at an angular frequency ω and modulation depth M . The resulting fluorescence signal is modulated at the same frequency and a modulation depth m . However, because the fluorescence is delayed in respect of the excitation, the fluorescence signal is phase-shifted by a phase angle ϕ and the modulation depth is decreased by a factor μ . For a single-exponent decay, such a frequency-domain technique can yield the values of fluorescence lifetime in real time, since both the measured phase shift,

$$\phi = \arctan(\omega\tau) , \quad (1)$$

and the decrease in modulation,

$$\mu \equiv m/M = \left(1 + \omega^2\tau^2\right)^{-1/2} , \quad (2)$$

explicitly depend only on the lifetime and frequency. Multiexponent decays result in more complex dependences of the phase shift and modulation depth on frequency. Note that in contrast to time-domain measurements, no accumulation of

multiple data and deconvolution of the decay kinetics are required. Additionally, frequency-domain measurements can be easily extended to frequencies well above the cut-off frequency of the source provided that the ac component of the fluorescence signal is still resolved. Finally, such fluorescence lifetime measurements are almost insensitive to temporal drift of the excitation source power and photodetector sensitivity, resulting in reduced maintenance of the sensors and no need in signal normalization.

2.3 Preparation of *Bacillus globigii* spores

Spores from *B. globigii* (also, *B. anthropaeus*) ATCC 9372 (BAG-Biologische Analysen System GmbH, Germany) were produced as described in Ref. 28. The bacteria were sporulated by incubation either in liquid or on solid modified Schaeffer's sporulation medium (2×SG)²⁹ at 37 °C for 3 days. Liquid cultures were incubated with vigorous aeration in a rotary shaker. Progress through sporulation was monitored microscopically by scoring for the presence of phase-bright spores and by measuring the percentage of cells in a culture that were capable of surviving a heat treatment (60°C for 30 min).

The liquid cultures or the washes of the growth from the agar surfaces with sterilized deionised water were harvested by centrifugation (10,000 g, 10 min, 4 °C), stored in a cold room, and the spores were purified by repeated rounds of centrifugation and washing with cold deionised water over a period of 1–2 weeks (the duration of washing depended upon the appearance of the supernatant and the spore pack). During the washing procedures, the spores were kept chilled. Cleaned spores were stored until use as suspensions of 10¹⁰ to 10¹¹ CFU/ml in deionised water at 4 °C protected from light. The viable titres of spore preparations were determined by serial 10-fold dilution in 0.1 M Na phosphate buffer (pH 7.0) and plating on 2×SG solidified with 2.0% agar. For fluorescence measurements, a dense spore suspension was spotted on a quartz glass and dried out in air at a temperature of –5 °C.

3. BIOAGENT DISCRIMINATION USING SPECTRAL AND EXCITATION FLUORESCENCE MEASUREMENTS

To demonstrate the applicability of deep-UV LEDs for discrimination of bacterial spores against common autofluorescent interferents, spectral measurements of fluorescence of *B. globigii* spores, ovalbumin, flour, cotton, paper, dust, and diesel fuels were performed for 280 nm and 340 nm excitation. These two excitation wavelengths are already established for fluorescence discrimination of hazardous agents against other common airborne interferents.^{11,12}

In this work, *B. globigii* dry washed spores prepared as described in Section 2.3 were used as a primary simulant of hazardous biological agent *B. anthracis*. To imitate a possible scatter of fluorescence features, a counterpart stimulant, dry spores of *B. subtilis* extracted from medication *Bactisubtil* capsules (Hoechst Marion Roussel, Romainville, France), were employed.

Bacterial spores contain natural autofluorophores, such as aromatic amino acids and coenzymes NADH and derivatives of flavins. Two different UV LED emission wavelengths can be used to selectively excite different autofluorophores.¹⁵ The 280-nm LED excites aromatic amino acids (tyrosine and tryptophane), which have fluorescence bands between 300 nm and 400 nm depending on local environment. The 340-nm LED excites NADH and derivatives of flavins (riboflavin, flavin adenine dinucleotide) with the fluorescence bands 460 nm and 530 nm, respectively. Fluorescence of the latter fluorophores is sensitive not only to the local environment but also to cell metabolism. The fluorescence bands can shift as a result of several phenomena, such as binding of ligands, protein-protein association or quenching by surrounding groups. These factors result in different spectral features of different kinds of bacterial spores, moreover, there exists a large scatter in the spectral features of a particular kind of spores.³⁰ However despite these differences, fluorescence spectra of any spores have common similarities exhibiting fluorescence bands at about 335 nm and 450 nm.

A number of various possible interferents were used in this study. Protein-based interferents were imitated by ovalbumin (stimulant of viral particles) and wheat flour (stimulant of high-protein-content food particles). Cellulose-based interferents were represented by purified cotton and different kinds of paper (copier paper, newspaper paper, and old yellowish envelope paper) that contain cellulose of different chemical treatment and age. Diesel fuels (both of winter

and summer brands) stood for hydrocarbon interferents. Finally, we employed dust extracted from the filter of an air conditioning (AC) system as a mixture of airborne particles common to an office environment.

Figure 3 shows fluorescence spectra of various samples under 340-nm LED excitation. Fluorescence spectra of spores of *B. globigii* (solid line) and *B. subtilis* (dashed line) are shown in Fig. 3a. The fluorescence spectrum of *B. globigii* consists two distinct bands peaked at 470 nm and 540 nm. The first one can be attributed to NADH fluorescence, while the second one is probably due to fluorescence of flavins. The spectrum of *B. subtilis* have one broad band peaked at 430 nm, that can be attributed to fluorescence of NADH in an inhomogeneous environment. Figure 3b shows fluorescence spectra of cotton (solid line) and different kinds of paper, copier paper (dashed line), newspaper paper (dotted line), and old envelope paper (dash-dotted line). The emission bands of cotton and different kinds of paper are seen to peak from 410 nm to 450 nm, a typical spectral range for cellulose containing materials.³¹ Figure 3c shows fluorescence of various brands of commercial diesels. The spectra of all kinds of diesels exhibit a long-wavelength tail of the fluorescence band peaked at 355 nm (see Fig. 4), which is due to aromatic hydrocarbons. Figure 3d shows fluorescence spectra of ovalbumin (solid line), flour (dashed line), and AC dust (dotted line). The fluorescence spectra of ovalbumin and flour are very similar and are peaked at 430 nm. The spectrum of AC dust shows a broad band peaked at about 450 nm and is very similar to those of cellulose-containing interferents (Fig. 3b).

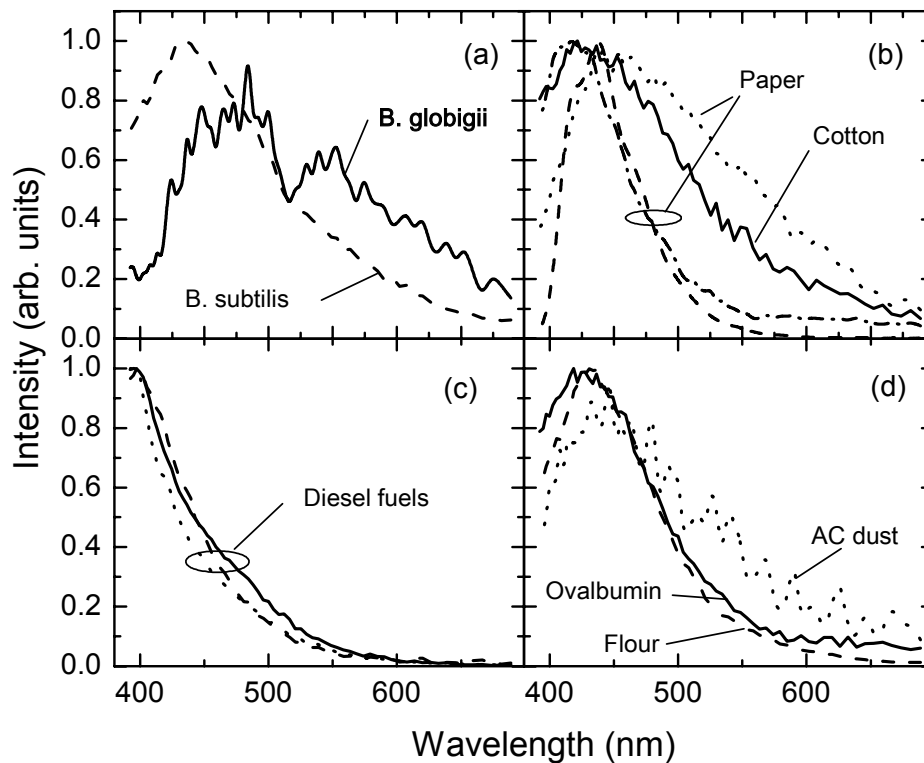


Fig. 3. 340-nm LED excited normalized fluorescence spectra of (a) bacterial spores *B. globigii* (solid line) and *B. subtilis* (dashed line); (b) cellulose-containing interferents cotton (solid line) and different kinds of paper (dashed, dotted, and dash-dotted lines); (c) diesel fuels; (d) protein-containing interferents ovalbumin (solid line) and flour (dashed line) and AC dust (dotted line).

Figure 3 shows that for 340-nm excitation, washed *B. globigii* spores exhibit a distinguishable spectrum with a characteristic dip at about 515 nm. However, analysis of the counterpart spectrum of *B. subtilis* indicates that discrimination of bacterial spores against most of interferents might be difficult (only diesel fuels exhibiting a high ratio of blue-to-red intensities can be spectrally discriminated). In practical detect-to-warn sensors containing a couple

detection channels with broad-band filters, spectral discrimination under 340-nm excitation would be even more ambiguous.

Using a 280 nm LED for excitation, more spectral features in the fluorescence spectra can be resolved, since aromatic amino acids (tryptophan and tyrosine) or aromatic hydrocarbons can be excited. Figure 4 shows fluorescence spectra of the studied samples under 280-nm excitation. Fluorescence spectra of *B. globigii* spores (solid line) and *B. subtilis* spores (dashed line) are shown in Fig. 4a. The fluorescence spectra of *B. globigii* now consists of three bands with the peaks at 320 nm, 463 nm and 550 nm. The new band in the UV part of the spectrum corresponded to protein aromatic amino acids, whereas the longer-wavelength bands are similar to those observed under 340-nm excitation. The spectrum of the counterpart spores of *B. subtilis* (dashed line in Fig. 4a) also contains a peak due to aromatic amino acids with a much lower ratio of the UV-to-blue emission intensities, however. Cotton and paper (Fig. 4b) exhibit spectra that are very similar to those obtained under 340-nm excitation (Fig. 3a). Note that the spectra feature a short-wavelength tail that in some cellulose-containing interferents is comparable in intensity with the UV band of *B. subtilis*. Figure 4c depicts the spectra of diesel fuels with a well-resolved peak at about 355 nm, which is due to aromatic rings of hydrocarbons. Similarly, the protein-containing interferents ovalbumin and flour (solid and dashed lines in Fig. 4d, respectively) contain a single band peaked at about 330 nm due to aromatic amino acids such as tryptophan residuals. Since under 280-nm LED excitation both hydrocarbons and protein-based interferents exhibit a high UV-to-blue intensity ratio, they can be easily distinguished from bacterial spores. Again, AC dust (dotted line in Fig. 4d) shows a spectrum very similar to cellulose-containing interferents (Fig. 4b).

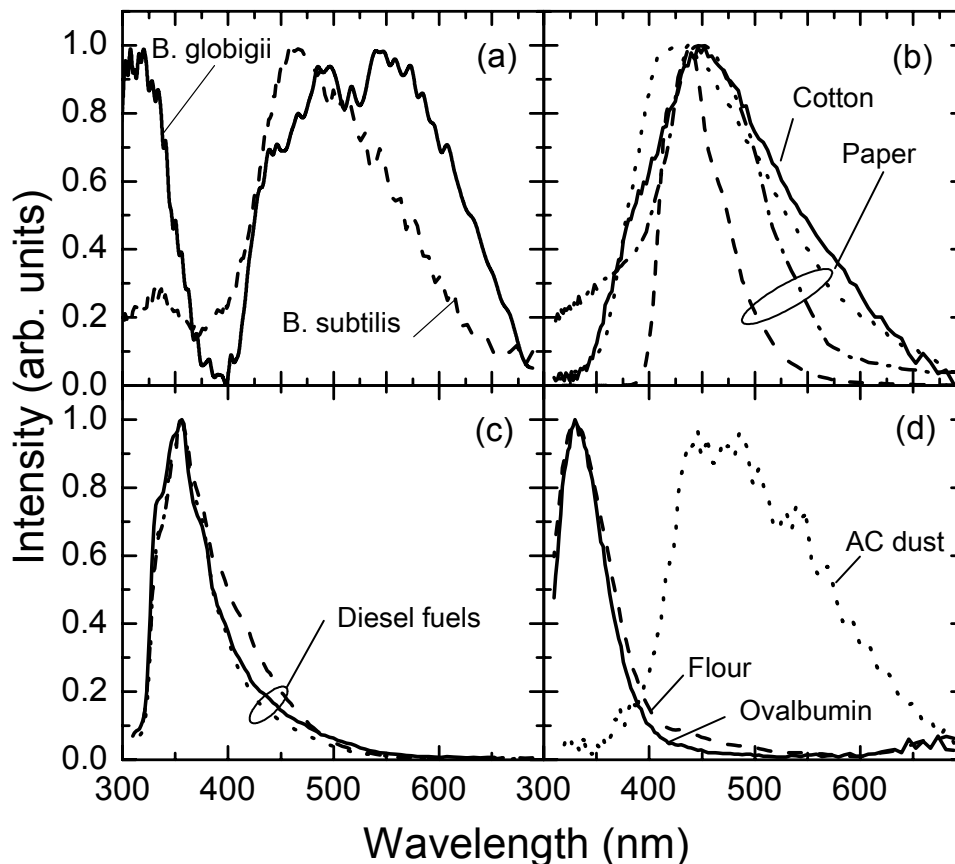


Fig. 4. 280-nm LED excited normalized fluorescence spectra of (a) bacterial spores *B. globigii* (solid line) and *B. subtilis* (dashed line); cellulose-containing interferents cotton (solid line) and different kinds of paper (dashed, dotted, and dash-dotted lines); (c) diesel fuels; (d) protein-containing interferents ovalbumin (solid line) and flour (dashed line) and AC dust (dotted line).

Comparison of Figs. 3 and 4 clearly indicates that the 280-nm LED excitation allows for an improved fluorescence discrimination of bacterial spores against most of interferents under study. Even using a simple two-channel detection system with UV and blue-green LPF filters (e. g. with the transmittance spectra shown in Fig. 2), aromatic hydrocarbons and high-protein-content interferents can be easily discriminated. However, cellulose-containing interferents and office dust are still difficult to distinguish because in some of these interferents the blue-band dominated spectra is contributed by residual UV emission.

To improve the discrimination ability of the fluorescence spectral measurements, we attempted to employ the fluorescence excitation characteristics. For just two excitation wavelengths utilized, such a characteristics can be represented by a difference in intensity of normalized spectra $\Delta(\lambda) = I_{280}(\lambda) - I_{340}(\lambda)$. Figure 5 depicts the differential spectra of the bacterial spores (a) and the interferents (b to d) obtained by subtracting the spectra shown in Fig. 3 from those corresponding shown in Fig. 4. (Note that under 340-nm excitation, the fluorescence intensity in the UV region is set to zero.) Vertical gray bars in Fig. 5 denote three characteristic wavelengths that were selected for improved discrimination: 320 nm (the peak of tryptophan emission), 405 nm (the dip in the spore spectra), and 566 nm (emission of flavins).

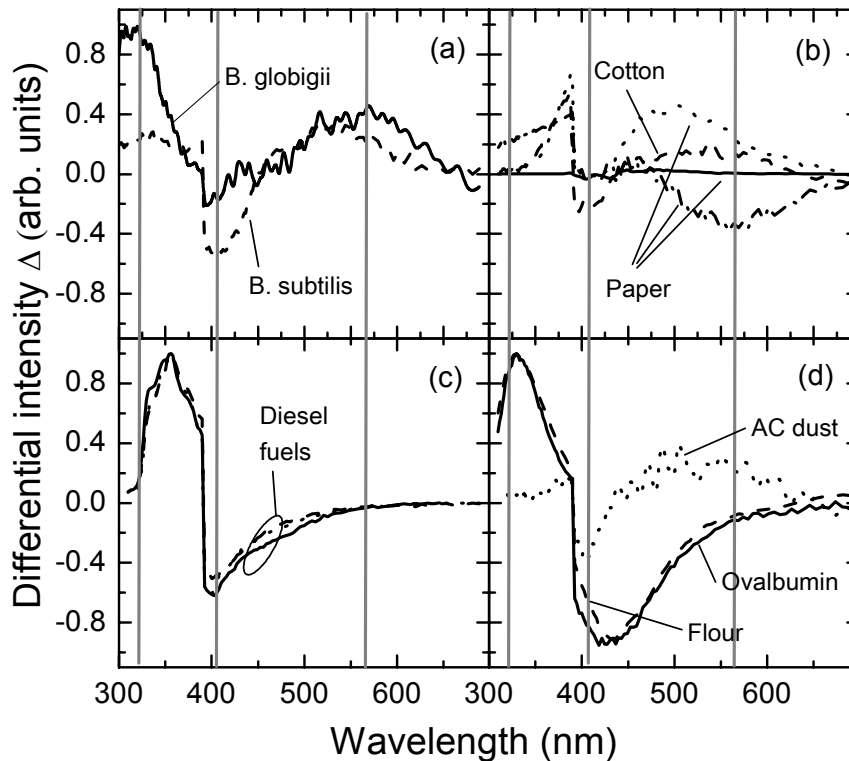


Fig. 5. Differential fluorescence spectra for 280 nm and 340 nm LED excitation of (a) bacterial spores *B. globigii* (solid line) and *B. subtilis* (dashed line); cellulose-containing interferents cotton (solid line) and different kinds of paper (dashed, dotted, and dash-dotted lines); (c) diesel fuels; (d) protein-containing interferents ovalbumin (solid line) and flour (dashed line) and AC dust (dotted line).

The differential spectra of *B. globigii* and *B. subtilis* spores (Fig. 5a) show positive values in the UV and green regions and a reduced or even negative intensity in the violet region. Such an excitation spectra signature remarkably differs from those of diesel fuels (Fig. 5c) and protein-based ovalbumin and flour (Fig. 5d), which show only negative values in the entire blue-green region. This makes the discrimination of bacterial spores against such interferents easy, since the discrimination can be based just on the sign of the differential spectrum. However again, cellulose-containing

interferents (Fig. 5b) and AC dust (dotted line in Fig. 5d) exhibit a diverse behavior that can hamper the discrimination when the bacterial spectrum differs from that of washed *B. globigii*.

The results of the fluorescence excitation analysis are summarized in Fig. 6. Here the differential intensities at 320, 405, and 566 nm are collated in two two-coordinate plots: $\Delta(320 \text{ nm})$ vs. $\Delta(405 \text{ nm})$ (Fig. 6a) and $\Delta(320 \text{ nm})$ vs. $\Delta(566 \text{ nm})$ (Fig. 6b). Figure 6a shows that in the 320/405 nm differential regime, a two-LED bioparticle sensor has a fair discrimination ability of bacterial spores against most of interferents (only *B. subtilis* point might be too close to the diesel fuel area). However operation of the detector at the 405-nm wavelength is unfavorable, since a narrow-band LPF is needed and the dip-like feature of the fluorescence spectrum in this region require a higher sensitivity.

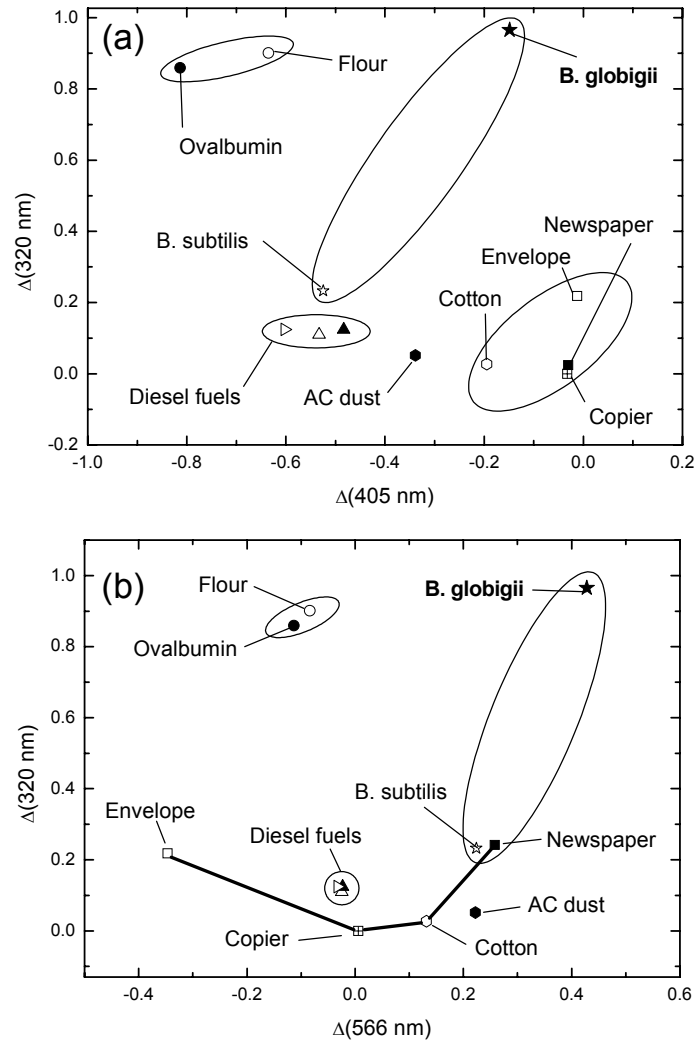


Fig. 6. Differential spectral response of fluorescence at 320 nm vs. 405 nm (a) and at 320 nm vs. 566 nm (b) for bacterial spores and various interferents.

In the case of 320/566 nm differential regime (Fig. 6b), which is more favorable in terms of the sensitivity of the detection system, the discrimination ability of a two-LED bioparticle sensor is lower. Although the point of the washed spores of *B. globigii* is still well resolved, the point of the counterpart stimulant *B. subtilis* falls into the vast region of cotton-containing interferents and probably dusts.

Based on the above analysis of the spectral and excitation data, as well on the extended data presented in literature (see, e.g., Refs. 11 and 30), one can conclude that a conventional two-excitation-wavelength (280/340 nm) system cannot provide sufficient discrimination of bacterial spores against some interferents using simple means of detection. We demonstrated that this especially applies for interferents containing cellulose (cotton, paper, and the relevant office dust), but we imply that problems with pollen, fungi, and some other interferents might be of the same or even higher importance.

Therefore, additional information on optical response from substances constituting aerosol microparticles is to be extracted. One of the possible routes in improving the discrimination ability of optical detect-to-warn sensors of bioparticles is the utilization of fluorescence lifetime as a supplementary parameter. Below we present the results of a tentative study on discrimination of bacterial spores against common interferents using this third dimension of fluorescence sensing.

4. FLUORESCENCE-LIFETIME DISCRIMINATION OF BACTERIAL SPORES AGAINST INTERFERENTS

Fluorescence lifetime is a fluorophore fingerprint, which in comparison with fluorescence intensity weakly depends on fluorophore concentration and is less subjected to photobleaching effect. Also, the lifetime measurements are less sensitive to temporal drift of the excitation source power and photodetector sensitivity, what allows for avoiding of normalization procedures and reducing maintenance of the sensors. Sensing of fluorescence lifetime makes possible to judge about the fluorophore environment. These advantages base numerous fluorescence lifetime sensors.^{7,15}

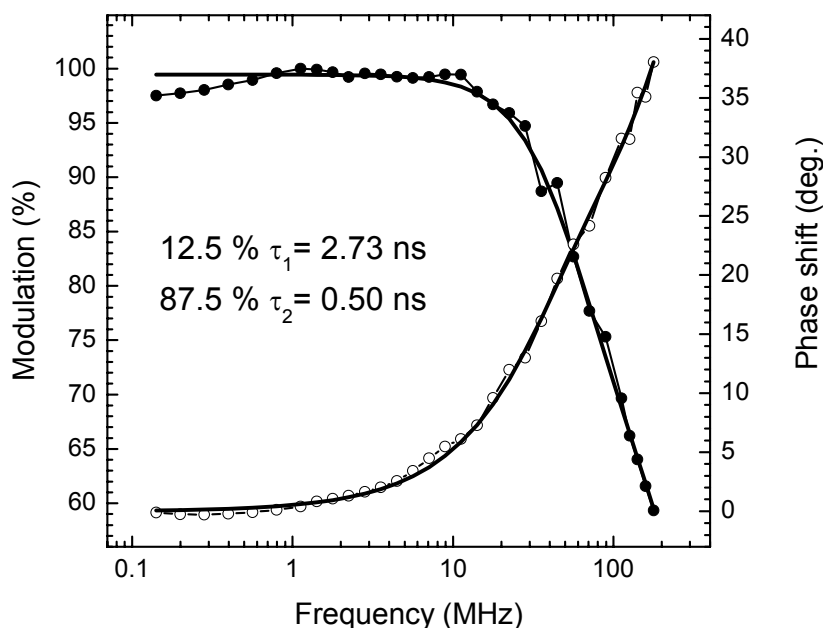


Fig. 7. Phase shift (open points) and modulation factor (solid points) as a function of frequency for *B. globigii* dry spores under UVTOP[®] series 280-nm LED excitation. Lines, the least-square fit to a two-exponent decay law.

Figure 7 shows the results of the fluorescence lifetime measurements for *B. globigii* spores in the frequency-domain obtained under 280-nm LED excitation. With increasing frequency, the phase shift between the harmonically modulated LED emission and the fluorescence increases, whereas the modulation depth decreases. Fitting (solid lines) of the experimental phase and modulation dependences vs. frequency (points) to a two-exponent fluorescence decay model by the least squares method revealed two fluorescence lifetimes: the main component (87.5%) is $\tau_1 = 0.5 \pm 0.1$ ns and the weaker component (12.5%) is $\tau_2 = 2.73 \pm 0.1$ ns. Note that the LPF used in the measurement (Fig. 2b) was tailored with

the emission of protein amino acids. Therefore, the shorter lifetime should be attributed to fast quenching processes in proteins due to inhomogeneous environment rather than to NADH. The longer fluorescence lifetime can be attributed to unquenched tryptophan residuals. Under 340-nm LED excitation, the component with $\tau_1 = 0.64 \pm 0.1$ ns dominates the decay (97.8%) and a weak contribution (2.2%) due to a longer lifetime $\tau_2 = 6.3 \pm 0.1$ ns can be resolved. These components are probably to NADH and flavins, respectively.²² It should be noted that the modulation factor and phase shift yield independent results, thus proving the reliability of the measurement.

Figure 8 shows the results of the frequency-domain fluorescence lifetime measurements for 340-nm LED excitation (a–d, left) and 280-nm LED excitation (e–h, right). (Only phase shift dependences are shown, since the modulation dependences yield no additional information.) The striking result is that bacterial spores and the interferences under study exhibit differences in the phase shift dependences that in many cases are out of line with the differences in the fluorescence spectra.

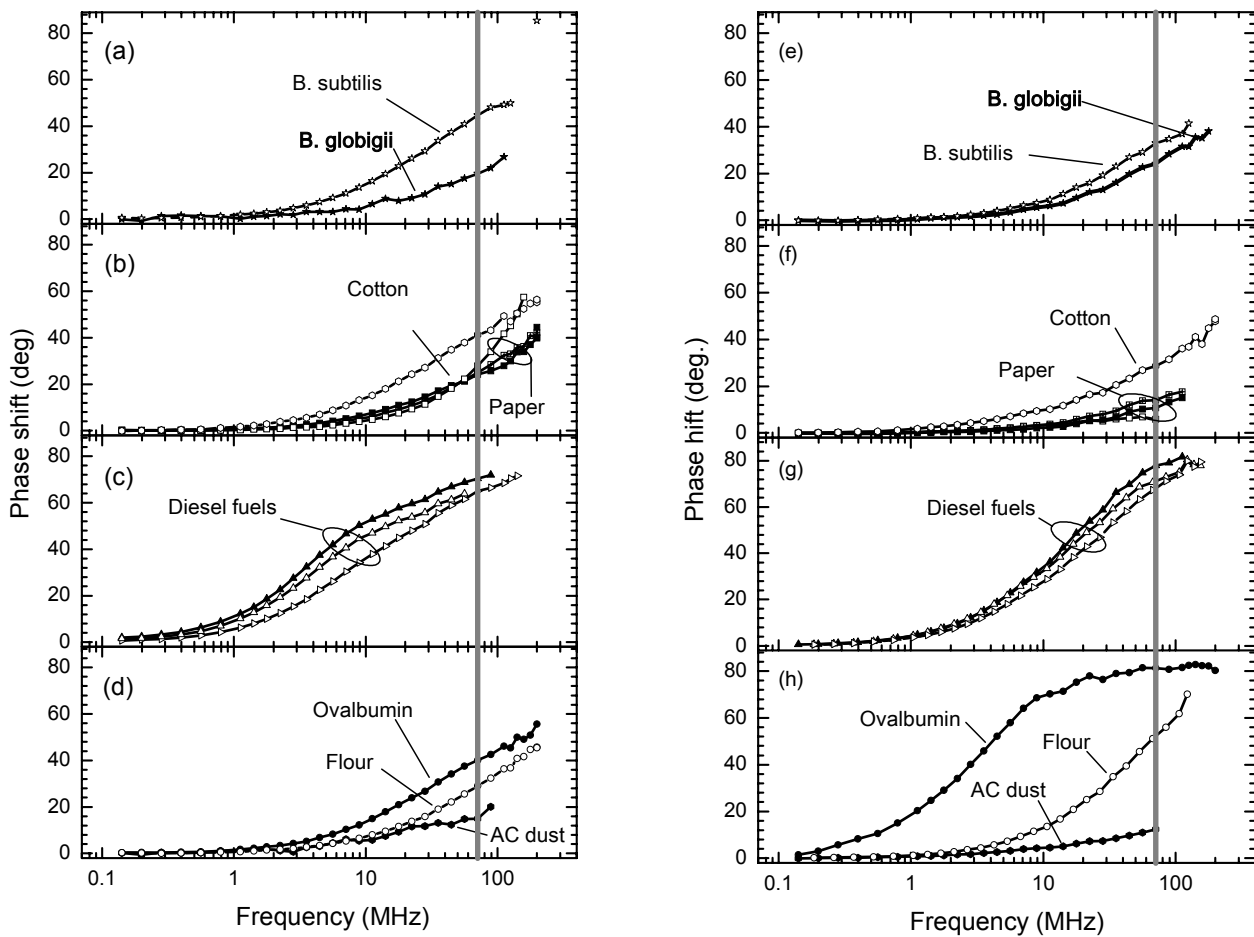


Fig. 8. Phase shift under 340-nm (left) and 280-nm (right) LED excitation as a function of frequency for (a, e) *B. globigii* spores (open stars) and *B. subtilis* (filled stars); (b, f) cotton (open hexagons) and different kinds of paper (squares); (c, g) diesel fuels (triangles); (d, h) ovalbumin (filled circles), flour (open circles), and AC dust (filled hexagons).

For instance, *B. globigii* and *B. subtilis* show quite different phase shifts under 340-nm excitation (Fig. 8a) and more similar phase shifts under 280-nm excitation (Fig. 8e), whereas the difference in fluorescence spectra is more pronounced for 340-nm excitation (see Figs. 3a and 4a). Again, cotton reveals a considerably larger phase shift (i.e.

longer fluorescence lifetime) than paper for both 340-nm and 280-nm excitation (Figs. 8b and f, respectively), whereas the fluorescence spectra of cotton falls within those of various kinds of paper (Figs. 3b and 4b). Contrarily, different kinds of paper that have highly dispersed features of fluorescence spectra (see Fig. 5b) with almost no dependence on the excitation wavelength exhibit very uniform phase shifts for each excitation wavelength with a remarkable decrease in fluorescence lifetime for 280-nm excitation (Figs. 8b and f). All diesel fuels have relatively large phase shifts evidencing large lifetimes (Figs. 8c and g). Again, ovalbumin and flour, which exhibit very similar fluorescence spectra (Figs. 3d and 4d), show completely different phase shifts (Figs. 8d and h). AC dust (Fig. 8d and 8h) have a phase dependence very similar to those of paper but very different from cotton (Fig. 8b and f).

To summarize the data on discrimination of the bacterial spores against interferents using fluorescence lifetime measurements, we plotted a two-coordinate diagram of the phase shifts at a single value of frequency (71 MHz). The plot (Fig. 9) presents the phase shift obtained at 340-nm excitation vs. the phase shift obtained under 280-nm excitation. We employed the phase shift at a particular frequency as the fingerprint of a substance rather than fluorescence lifetime, since some substances exhibited multiexponential decays. Also, the phase shift is the directly measured quantity that can be used in real-time sensing. The frequency of 71 MHz (gray vertical bars in Fig. 8) was chosen as an optimal one for such real-time measurements.

Figure 9 indicates that such interferents as diesel fuels and high-protein-content interferents (ovalbumin and flour) can be easily distinguished from bacterial spores even using a single-channel fluorescence lifetime sensing (for 280-nm excitation only). Paper particles and AC dust are also well-discriminated against bacterial spores at 280-nm excitation due to a large difference in phase shift. The most persistent interferent of those investigated is cotton, which has a point in between those of bacterial spores. Fortunately, cotton can be discriminated based on fluorescence spectral features (see, e.g., Fig. 6b).

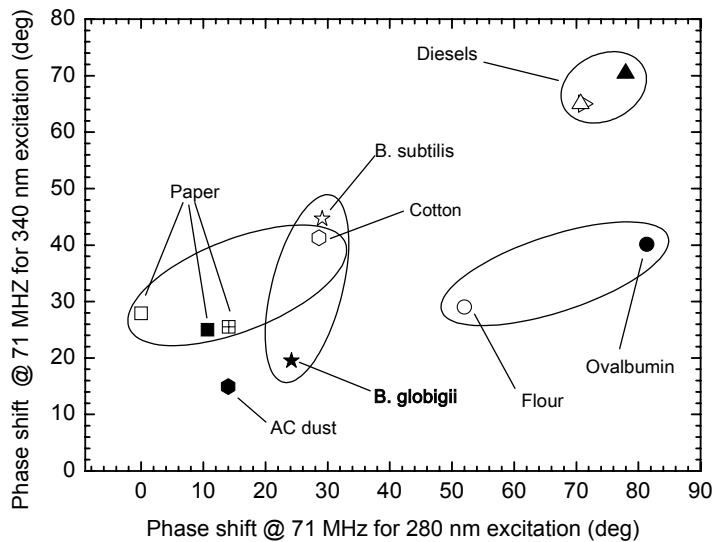


Fig. 9. Distribution of the 340-nm excited fluorescence phase shift at 71 MHz vs. the 280-nm excited fluorescence phase shift at 71 MHz for the bacterial spores and interferents under study.

The above comparison of spectral and lifetime features of bacterial spores and common interferents clearly indicates that fluorescence lifetime measurements provide with non-trivial information on the substances contained in airborne particles. This grounds the use of fluorescence lifetime measurements as a third dimension for improved discrimination of airborne bacterial spores against interferents. We expect that fluorescence lifetime data for similar objects should exhibit a lower scatter in comparison with the spectral data, since fluorescence lifetime is an absolute fingerprint of a fluorophore, which does not depend on concentration of particles, temperature and aging drift of the power of the excitation source and of the photodetector sensitivity, contamination of optical elements, etc.

5. CONCLUSIONS

In conclusion, we applied 340-nm and 280-nm LEDs developed by Sensor Electronic Technology, Inc. for fluorescence discrimination of bacterial spores (*B. globigii* and *B. subtilis*) against substances contained in common airborne interferents, such as paper, cotton, diesel fuels, high-protein content products (ovalbumin and flour), and office dust trapped in air conditioning system. Conventional two-channel spectral and excitation fluorescence discrimination using 280-nm and 340-nm LEDs was shown to be insufficient for operating of the detect-to-warn optical sensors of bioparticles at a low false alarm rate. To mitigate this drawback, we introduced fluorescence lifetime measurements that employ the same deep-UV LEDs. The measurements were carried out in the frequency domain mode, which allows real-time characterization of fluorophors by measuring the phase shift between the harmonically modulated excitation and fluorescence. The phase shift measured at about 70 MHz was shown to provide with non-trivial information on fluorescence decay that can be used as an additional dimension in fluorescence-based identification of substances contained in aerosol particles. We conclude that fluorescence lifetime, which is an absolute fingerprint of a fluorophore, can supplement the spectral and excitation data on fluorescence of bacterial spores and common interferents and a substantial improvement of the discrimination ability of detect-to-warn sensors of airborne bioparticles can be anticipated.

However, we recognize that present technology of cost-efficient fluorescence lifetime measurements lack sensitivity and cannot be used for single particle interrogation. Therefore further work on improvement of real-time measurement technology for sensitive measuring of fluorescence lifetime in-real time is required. Nevertheless, fluorescence lifetime measurements in the frequency domain can be already tested in sensors that employ aerosol concentration, e.g., by collection on a surface.¹⁰

ACKNOWLEDGEMENTS

The work was supported by the Lithuanian State Science and Studies Foundation under COST action No 529 and NanoBioPolymers program (grant No C-18/2003) and by the SELITEC Center supported by the European Commission (contract No.G5MA-CT-2002-04047).

REFERENCES

1. J. C. Carrano and A. J. Maltenfort, "Semiconductor ultraviolet sources for biological agent detection," *Proc. SPIE* **4743**, pp. 261–267, 2002.
2. see papers in *Optically Based Biological and Chemical Sensing for Defence*, ed. by J. C. Carrano and A. Žukauskas, *Proc. SPIE* **5617**, 2004.
3. R. G. Pinnick, S. C. Hill, S. Niles, D. M. Garvey, Y.-L. Pan, S. Holler, R. K. Chang, J. Bottiger, B. V. Bronk, B. T. Chen, C.-S. Orr, and G. Feather, "Real-time measurement of fluorescence spectra from single airborne biological particles," *Field Anal. Chem. Technol.* **3**, pp. 221–239, 1999.
4. V. Sivaprakasam, A. L. Huston, C. Scotto, and J. D. Eversole, "Multiple UV wavelength excitation and fluorescence of bioaerosols," *Optics express* **12**, pp. 4457–4466, 2004.
5. P. Jonsson, F. Kullander, M. Nordstrand, T. Tjærnhage, P. Wästerby and M. Lindgren, "Development of fluorescence-based point detector for biological sensing," *Proc. SPIE* **5617**, pp. 60–74, 2004.
6. *UV Solid-State Light Emitters and Detectors*. Proc. NATO ARW, Series II, Vol. 144, ed. by M. S. Shur and A. Žukauskas, Kluwer, Dordrecht, 2004.
7. T. H. Jeys, L. Desmarais, E. J. Lynch, and J. R. Ochoa, "Development of a UV LED based biosensor," *Proc. SPIE* **5071**, pp. 234–240, 2003.
8. C. Call and E. Merrill, "AirSentinel[®]: A real-time bioaerosol monitor," *Proc. SPIE* **5617**, pp. 53–59, 2004.
9. J. Cabalo, R. Sickenberger, W. Underwood, and D. Sickenberger, "Micro-UV detector," *Proc. SPIE* **5617**, pp. 75–86, 2004.
10. R. DeFreez, E. Merrill, S. Albanna, B. Davis, and C. Call, "Design considerations and performance characteristics of AirSentinel[®], a new UV-LIF bio-aerosol threat detection trigger," *Proc. SPIE* **5990**, 2005.

11. P. H. Kaye, E. Hirst, V. Foot, J. M. Clark, and K. Baxter, "A low-cost multi-channel aerosol fluorescence sensor for networked deployment," *Proc. SPIE* **5617**, pp. 388–398, 2004.
12. S. D. Campbell, D. P. Tremblay, F. Daver, and D. Cousins, "Multiwavelength bioaerosol sensor performance modeling," *Proc. SPIE* **5990**, 2005.
13. J. D. Hybl, G. A. Lithgow, S. G. Buckley, "Laser-induced breakdown spectroscopy detection and classification of biological aerosols," *Appl. Spectrosc.* **57**, pp. 1207–1215 (2003).
14. M. C. Storr-Lombardi, W. F. Hug, G. D. McDonald, A. I. Tsapin, and K. H. Nealon, "Hollow cathode ion lasers for deep ultraviolet Raman spectroscopy and fluorescence imaging," *Rev. Sci. Instrum.* **72**, pp. 4452–4459, 2001.
15. J. R. Lakowicz, *Principles of Fluorescence Spectroscopy*, Kluwer Academic/Plenum, New York, 1999.
16. T. Araki and H. Misawa, "Light emitting diode-based nanosecond ultraviolet light source for fluorescence lifetime measurements," *Rev. Sci. Instrum.* **66**, pp. 5469–5472, 1995.
17. J. Sipior, G. M. Carter, J. R. Lakowicz, and G. Rao, "Single quantum well light emitting diodes demonstrated as excitation sources for nanosecond phase-modulation fluorescence lifetime measurements," *Rev. Sci. Instrum.* **67**, pp. 3795–3798, 1996.
18. H. Peng, E. Makarona, Y. He, Y.-K. Song, A. V. Nurmikko, J. Su, Z. Ren, M. Gherasimova, S.-R. Jeon, G. Cui, and J. Han, "Ultraviolet light-emitting diodes operating in the 340 nm wavelength range and application to time-resolved fluorescence spectroscopy," *Appl. Phys. Lett.* **85**, pp. 1436–1438, 2004.
19. C. D. McGuinness, K. Sagoo, D. McLoskey and D. J. S. Birch, "A new sub-nanosecond LED at 280 nm: application to protein fluorescence," *Meas. Sci. Technol.* **15**, pp. L19–L22, 2004.
20. P. Vitta, N. Kurilcik, A. Novickovas, S. Jursenas, H. Calkauskas, A. Žukauskas, and R. Gaska, "AlGaIn-based deep UV LEDs for fluorescence sensing," *Proc. SPIE* **5617**, pp. 249–260, 2004.
21. C. D. McGuinness, K. Sagoo and D. McLoskey, D. J. S. Birch, "Selective excitation of tryptophan fluorescence decay in proteins using a subnanosecond 295 nm light-emitting diode and time-correlated single-photon counting," *Appl. Phys. Lett.* **86**, 261911, 2005.
22. P. Vitta, N. Kurilcik, S. Juršėnas, A. Žukauskas, A. Lunev, Y. Bilenko, J. Zhang, X. Hu, J. Deng, T. Katona, and R. Gaska, "Deep-ultraviolet light-emitting diodes for frequency domain measurements of fluorescence lifetime in basic biofluorophores," *Appl. Phys. Lett.* **87**, 084106, 2005.
23. J. P. Zhang, A. Chitnis, V. Adivarahan, S. Wu, V. Mandavilli, R. Pachipulusu, M. Shatalov, G. Simin, J. W. Yang, and M. Asif Khan, "Milliwatt power deep ultraviolet light-emitting diodes over sapphire with emission at 278 nm," *Appl. Phys. Lett.* **81**, pp. 4910–4912, 2002.
24. V. Adivarahan, S. Wu, J. P. Zhang, A. Chitnis, M. Shatalov, V. Mandavilli, R. Gaska, M. A. Khan, "High-efficiency 269 nm emission deep ultraviolet light-emitting diodes," *Appl. Phys. Lett.* **84**, pp. 4762–4764, 2004.
25. W. H. Sun, J. P. Zhang, V. Adivarahan, A. Chitnis, M. Shatalov, S. Wu, V. Mandavilli, J. W. Yang, and M. A. Khan, "AlGaIn-based 280 nm light-emitting diodes with continuous wave powers in excess of 1.5 mW," *Appl. Phys. Lett.* **85**, pp. 531–533, 2004.
26. J. P. Zhang, X. Hu, Yu. Bilenko, J. Deng, A. Lunev, M. S. Shur, R. Gaska, M. Shatalov, J. W. Yang, and M. A. Khan, "AlGaIn-based 280 nm light-emitting diodes with continuous-wave power exceeding 1 mW at 25 mA," *Appl. Phys. Lett.* **85**, pp. 5532–5534, 2004.
27. P. Harms, J. Sipior, N. Ram, G. M. Carter, and G. Rao, "Low cost phase-modulation measurements of nanosecond fluorescence lifetimes using a lock-in amplifier," *Rev. Sci. Instrum.* **70**, pp. 1535–1539, 1999.
28. W. L. Nicholson and P. Setlow, "Sporulation, germination and out-growth," in *Molecular biological methods for Bacillus*, ed. by C. R. Harwood and S. M. Cutting, Wiley, Chichester, 1990, pp. 391–450.
29. T. J. Leighton and R. H. Doi, "The stability of messenger ribonucleic acid during sporulation in *Bacillus subtilis*," *J. Biol. Chem.* **246**, pp. 3189–3195, 1971.
30. P. H. Kaye, W. R. Stanley and E. Hirst, E. V. Foot, K. L. Baxter, and S. J. Barrington, "Single particle multichannel bio-aerosol fluorescence sensor," *Optics express* **13**, pp. 3583–3593, 2005.
31. J. A. Olmstead and D. G. Gray, "Fluorescence spectroscopy of cellulose, lignin, and mechanical pulps: A review," *J. Pulp Paper Sci.* **23**, pp. J571–J581, 1997.